Available online at www.sciencedirect.com

ScienceDirect

Mendeleev Commun., 2022, **32**, 129–131

Mendeleev Communications

Effect of the oxidizing capacity of ceria-based support on the conversion of methane to syngas

Igor V. Zagaynov,*[a] Alexey S. Loktev,[b,c] Igor E. Mukhin,[c] Anatoly A. Konovalov[a] and Alexey G. Dedov[b,c]

[a] *A. A. Baikov Institute of Metallurgy and Materials Science, Russian Academy of Sciences, 119991 Moscow, Russian Federation. E-mail: igorscience@gmail.com*

[b] *A. V. Topchiev Institute of Petrochemical Synthesis, Russian Academy of Sciences, 119991 Moscow, Russian Federation*

[c] *I. M. Gubkin Russian State University of Oil and Gas, 117917 Moscow, Russian Federation*

DOI: 10.1016/j.mencom.2022.01.042

Ceria-based solid solutions have been proposed as catalytic supports for the conversion of methane to syngas. Control of oxygen vacancies in vacancy-rich oxides represents a promising way to stable catalysts with improved activity.

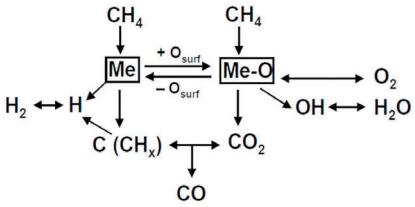

Keywords: ceria, solid solution, support, partial oxidation of methane, dry reforming of methane, syngas.

Conversion of methane to syngas (or synthesis gas, H_2 + CO), including the steam reforming of methane (SRM) and the dry reforming of methane (DRM), represents an endothermic and, therefore, energy intensive process. SRM gives a product with a high ratio of syngas H_2/CO = 3 suitable for the generation of ammonia, while DRM results in a lower syngas ratio of 1 appropriate for the synthesis of oxygenates. Contrary to that, the partial oxidation of methane (POM) as a technology aimed to increase the efficiency of syngas production has the ratio of syngas equal to 2, which represents an advantage in its further processing into methanol and liquid hydrocarbons (Fischer–Tropsch).[1–4] Considering thermodynamics, the optimal conditions for implementation of methane oxidation are the following: the gas mixture pressure equal to 1 atm and the temperature of 800–950 °C, while in terms of kinetics, the desired flow rate is up to 50000 h^{-1}. Under these conditions the methane conversion of >90% and the H_2 content of 50–60% in the resulting gaseous mixture ensure efficient further processing of the products.[5–8] A catalytic support should have a surface suitable for fixation of an active component of the catalyst. Common supports like oxides of Al, Mg, Si and Ti have a number of drawbacks leading to a decrease in catalytic activity due to sintering of an active component as well as coking.[9] Ceria-based solid solutions represent an alternative support,[10–12] the resulting catalysts have suitable redox properties, oxygen mobility and oxygen storage capacity (OSC), since the catalyst deactivation typically occurs quickly without noticeable oxygen mobility.[13] Though the thermal stability of pure ceria under typical reforming conditions is rather low, it can be improved by doping.[14–16] Besides, the use of mesoporous structures can further improve the characteristics of catalysts due to an increase in surface area, which may be associated with the effect of limitation of the sintering and agglomeration of active metal particles in the mesopores.[10,17] In this work, we investigated an effect of the Ce partial substitution in the ceria-based support on the catalytic properties of catalyst samples, which comprised supports or the active component–support systems, in the conversion of methane to syngas.

The main characteristics of the synthesized catalysts are collected in Table 1. The consideration of the complex supports originates from a need to stabilize the ceria structure for operations above 700 °C as well as from the known data on the influence of various dopants and their ratios on the catalytic properties,[10,18,19] as a result the best systems have been selected for further comparison. All the nanocrystalline compositions investigated have a developed surface and a mesoporous structure. From XRD patterns of the fresh catalysts

Table 1 Main characteristics of the fresh catalysts.

Sample no.	Composition	d_{XRD}/nm for the support	S_{BET}/ $m^2\ g^{-1}$	D_{pore}/nm
1	$Gd_{0.1}Ti_{0.1}Zr_{0.1}Ce_{0.7}O_2$	9	83	2–8
2	NiCoMn[a]–$Gd_{0.1}Ti_{0.1}Zr_{0.1}Ce_{0.7}O_2$	7	88	2–15
3	$Cu_{0.08}Mn_{0.02}Ce_{0.9}O_2$	9	79	2–25
4	NiCoMn[a]–$Cu_{0.08}Mn_{0.02}Ce_{0.9}O_2$	7	91	2–10
5	$Cu_{0.08}Mn_{0.02}Zr_{0.1}Ce_{0.8}O_2$	8	31	2–25
6	NiCoMn[a]–$Cu_{0.08}Mn_{0.02}Zr_{0.1}Ce_{0.8}O_2$	6	105	2–8
7	$Cu_{0.08}Mn_{0.02}Sm_{0.05}Ce_{0.85}O_2$	10	86	2–18
8	NiCoMn[a]–$Cu_{0.08}Mn_{0.02}Sm_{0.05}Ce_{0.85}O_2$	7	80	2–8
9	$Cu_{0.08}Mn_{0.02}Sm_{0.05}Zr_{0.1}Ce_{0.8}O_2$	7	83	2–18
10	NiCoMn[a]–$Cu_{0.08}Mn_{0.02}Sm_{0.05}Zr_{0.1}Ce_{0.8}O_2$	5	94	2–8

[a] 5 wt% NiCoMn with Ni/Co/Mn = 72 : 18 : 10 mol.

[Figure S1(*a*), Online Supplementary Materials] it is clear that the supports have been synthesized correctly relative to the active component. Diffraction peaks of the support and the active component phases with a cubic structure are observed. The peaks at *ca.* 37.3 and 43.3° are generally related to the NiO phase, however, due to the shift of the peak, they are more likely attributed to the formation of the cubic phase of NiCoMnO.

The average crystallite size, calculated using the Scherrer equation, is 5–10 nm (see Table 1) and according to TEM the nanoparticle size is 4–15 nm (Figure S2).

For the assessment of redox properties and mobility of oxygen ions in the ceria lattice, the oxidation of CO is typically used.[20] The conversion of CO increases with temperature, the corresponding curves being S-shaped [Figure 1(*a*)]. When metal oxides are added to ceria, the catalytic activity in the CO oxidation elevates due to a synergistic effect, which is most significant after the Mn and/or Cu addition,[18,19] in this way the samples 3 and 7 represent the most active supports. Transition metal oxides have multivalent oxidation states that allow the material to donate lattice oxygen for a reaction with adsorbed molecules, the catalytic surface being subsequently reoxidized by the gas phase oxygen. Therefore, with these oxide catalysts, the oxidation reactions are supposed to follow the Mars–van Krevelen mechanism, according to which the molecules are oxidized by consuming lattice oxygen of the oxide catalyst, which is in turn reoxidized. However, CO oxidation occurs in the intermediate temperature range, while methane is oxidized at higher temperatures [T > 750 °C, Figure 1(*b*)–(*d*)], where the activity is shifted to the systems stabilized by Zr, because ceria has low thermal stability and sinters during the process. As the sintering occurs due to crystallite growth, it could be said that Zr improves the thermal stability of ceria by decreasing the rate of the crystallite growth. The most active supports are the samples 5 and 9 both in the POM and DRM reactions.

Activity of the catalysts (see Figure 1) and the product selectivity (Figure 2) in the POM and DRM processes both increase with temperature, at 950–975 °C they reach maximum values and further elevation to >1000 °C leads to lowering of the parameters measured. Considering the active phase, the corresponding samples exhibit high catalytic activity, the best

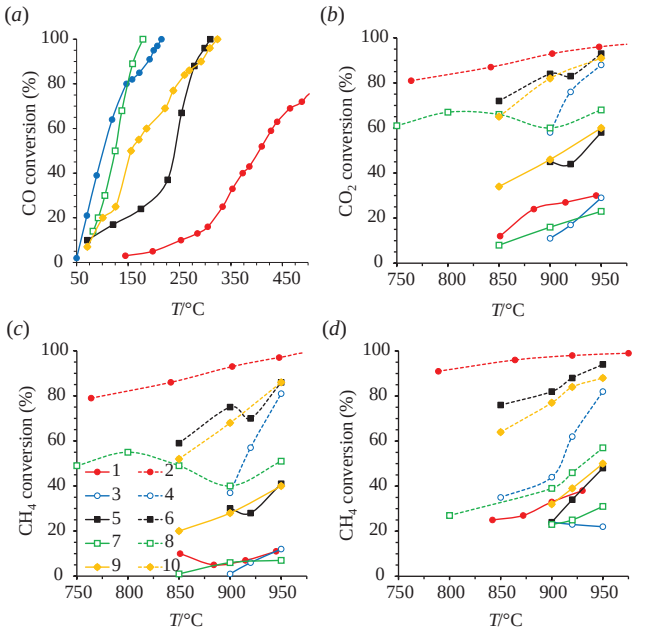

Figure 1 Activity of the catalyst samples in (*a*) CO oxidation, (*b*,*c*) DRM and (*d*) POM.

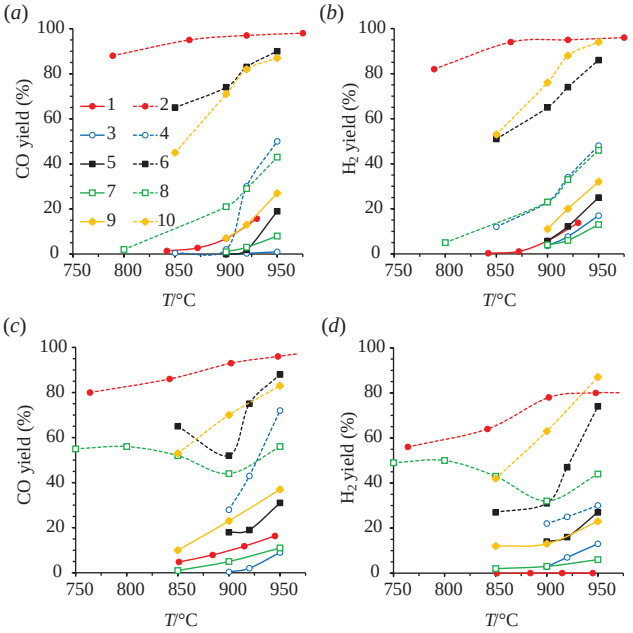

Figure 2 Product yield *vs.* temperature for (*a*,*b*) POM and (*c*,*d*) DRM.

results have been obtained for the sample 2, which has the support with a lower oxidative activity.

Ceria itself is catalytically active in the oxidation of methane. It is known[21,22] that ceria is able to convert methane directly to syngas at >600 °C. This indicates that the creation of an oxygen vacancy and structure distortion increase the migration of lattice oxygen and the content of surface oxygen species. This lattice-activated oxygen has a tendency to facilitate the partial oxidation of methane. Likewise, it has been reported that there are two types of oxygen for the processes on oxides, namely the surface adsorbed one, which contributes to the complete combustion of methane to form CO_2 and H_2O, and the bulk lattice oxygen, which favors the formation of CO and H_2.[23] The reducible oxides help in enhancing catalytic activity and stability:

$$O_2(CO_2)+V_{\ddot{O}} \rightarrow O^{2-} \rightarrow O^{2-}\text{ back-spillover} \rightarrow$$
$$\rightarrow O^{\delta-}\text{//NiCoMnO} \leftrightarrow \text{NiCoMn//}CH_4 \rightarrow CH_x. \quad (1)$$

Existing oxygen vacancies of the ceria lattice are ‘healed’ by an oxidizing agent like oxygen or CO_2, thus forming oxygen ions. Further, the oxygen ions are transferred from support to the active phase by the back-spillover process oxidizing the metal support or the metal−C system. In turn, the oxidized active phase is reduced to the metallic state or the metal−C system with methane. The oxygen vacancy formation begins through the direct participation of available lattice oxygen species in the C−H bond activation. According to Raman data, the oxygen vacancies are present in supports even before the catalytic tests.[18,19] However, highly reactive oxygen has been shown to be disadvantageous, when there is an active component in the form of NiCoMn, thus the superiority of the sample 2 is affected, though in this case the supports 5 and 9 can be used without an active component. The Boudouard reaction ($2CO \rightleftharpoons CO_2 + C$) and methane decomposition represent two major pathways for carbon formation at high temperatures. The resistance toward carbon deposition for a ceria solid solution originates from a high OSC value.[24,25] Using ceria-based systems, the reactions of carbon formation can be inhibited by redox processes with lattice oxygen at the support surface. The addition of Zr can not only enhance the thermal stability of a material, but also promote an increase in oxygen vacancy amount in the catalyst during the redox process.[26,27] The catalysts 5 and 9 reveal relatively high catalytic activity and stability in the redox experiment for the

successive generation of syngas. This property is associated with the increased oxygen vacancies located on the surface and in the bulk of catalyst after cycling, which strongly enhances the lattice oxygen mobility. This behavior would counteract the negative effect of catalyst sintering on the catalytic activity of the material for methane conversion. XRD patterns of the used catalysts [Figure S1(*b*)] indicate that the diffraction peaks of NiCoMnO and/or NiCoMn phases as well as the phase of ceria-based support are still present. The formation of other phases like carbides, spinel or perovskite has not been observed, thus the proposed catalysts are highly stable.

In this work, ceria-based solid solutions were prepared by coprecipitation, characterized by physicochemical techniques and investigated in the catalytic conversion of methane, namely the POM and DRM processes. It was shown that the nature and the composition of dopants influenced the redox properties and catalytic activity. The amount of lattice oxygen in these catalysts taking part in the oxidation reactions increases with temperature due to elevation of oxygen mobility in the oxide lattice. For the selective conversion of methane, in contrast to the complete oxidation of CO, a metered amount of active oxygen is required, which differs in the binding energy in the oxide lattice in conjunction with the presence of an active phase.[28–30] There are two types of mobile lattice oxygen in the catalyst sample, namely weakly and strongly bound oxygen atoms, so to enhance the selectivity it is necessary to decrease the content of 'nonselective' oxygen in the support. However, the samples $Cu_{0.08}Mn_{0.02}Zr_{0.1}Ce_{0.8}O_2$ and $Cu_{0.08}Mn_{0.02}Sm_{0.05}Zr_{0.1}Ce_{0.8}O_2$ (5 and 9) can be employed directly without an active Ni-containing component for the methane conversion with no coking. Improving the amount of the surface active oxygen sites represents the major reason accounting for the enhanced reaction performance and coking resistance of the catalysts. The ability to control the content of the oxygen vacancies in the lattice and homogeneously dispersed active particles on the support will be beneficial in the design of stable catalysts with improved activity.[31]

This work was partially supported by the Ministry of Science and Higher Education of the Russian Federation within the governmental orders and the state funding of the A. A. Baikov Institute of Metallurgy and Materials Science, Russian Academy of Sciences (BET–BJH) and the A. V. Topchiev Institute of Petrochemical Synthesis, Russian Academy of Sciences (the DRM experiments).

Online Supplementary Materials

Supplementary data associated with this article can be found in the online version at doi: 10.1016/j.mencom.2022.01.042.

References

1 V. S. Arutyunov and O. V. Krylov, *Russ. Chem. Rev.*, 2005, **74**, 1111 (*Usp. Khim.*, 2005, **74**, 1216).
2 I. V. Zagaynov, *Energy Fuels*, 2021, **35**, 9124.
3 A. M. Ranjekar and G. D. Yadav, *J. Indian Chem. Soc.*, 2021, **98**, 100002.
4 L. V. Sineva, E. O. Gorokhova, E. V. Kulchakovskaya, E. Yu. Asalieva, E. A. Pushina, A. N. Kirichenko and V. Z. Mordkovich, *Mendeleev Commun.*, 2020, **30**, 198.
5 S. H. Chan, O. L. Ding and D. L. Hoang, *Int. J. Green Energy*, 2004–2005, **1**, 265.
6 S. Kumar, S. Kumar and J. K. Prajapati, *Int. J. Hydrogen Energy*, 2009, **34**, 6655.
7 W.-H. Chen, H.-J. Liou and C. I. Hung, *Int. J. Hydrogen Energy*, 2013, **38**, 5270.
8 R. Y. Chein, W. H. Hsu and C. T. Yu, *Int. J. Hydrogen Energy*, 2017, **42**, 14485.
9 X. Zhu, H. Wang, Y. Wei, K. Li and X. Cheng, *J. Nat. Gas Chem.*, 2011, **20**, 281.
10 I. V. Zagaynov, A. S. Loktev, A. L. Arashanova, V. K. Ivanov, A. G. Dedov and I. I. Moiseev, *Chem. Eng. J.*, 2016, **290**, 193.
11 I. V. Zagaynov, A. S. Loktev, I. E. Mukhin, A. G. Dedov and I. I. Moiseev, *Mendeleev Commun.*, 2017, **27**, 509.
12 I. V. Zagaynov, A. S. Loktev, I. E. Mukhin, A. A. Konovalov, A. G. Dedov and I. I. Moiseev, *Mendeleev Commun.*, 2019, **29**, 22.
13 K. Chang, H. Zhang, M.-j. Cheng and Q. Lu, *ACS Catal.*, 2020, **10**, 613.
14 Y. Bespalko, E. Smal, M. Simonov, K. Valeev, V. Fedorova, T. Krieger, S. Cherepanova, A. Ishchenko, V. Rogov and V. Sadykov, *Energies*, 2020, **13**, 3365.
15 B. Safavinia, Y. Wang, C. Jiang, C. Roman, P. Darapaneni, J. Larriviere, D. A. Cullen, K. M. Dooley and J. A. Dorman, *ACS Catal.*, 2020, **10**, 4070.
16 A. Salcedo, I. Iglesias, F. Mariño and B. Irigoyen, *Appl. Surf. Sci.*, 2018, **458**, 397.
17 C. Ding, W. Liu, J. Wang, P. Liu, K. Zhang, X. Gao, G. Ding, S. Liu, Y. Han and X. Ma, *Fuel*, 2015, **162**, 148.
18 I. V. Zagaynov, I. V. Shelepin, S. V. Fedorov, A. V. Naumkin, A. V. Bykov and A. A. Konovalov, *Ceram. Int.*, 2021, **47**, 22201.
19 I. V. Zagaynov, A. V. Naumkin and Y. V. Grigoriev, *Appl. Catal., B*, 2018, **236**, 171.
20 *Catalysis by Ceria and Related Materials*, 2nd edn., eds. A. Trovarelli and P. Fornasiero (*Catalytic Science Series*, ed. G. J. Hutchings, vol. 12), Imperial College Press, 2013.
21 K. Otsuka, T. Ushiyama and I. Yamanaka, *Chem. Lett.*, 1993, **22**, 1517.
22 K. Otsuka, Y. Wang, E. Sunada and I. Yamanaka, *J. Catal.*, 1998, **175**, 152.
23 X. Lin, S. Li, H. He, Z. Wu, J. Wu, L. Chen, D. Ye and M. Fu, *Appl. Catal., B*, 2018, **223**, 91.
24 E. V. Matus, D. V. Nefedova, V. V. Kuznetsov, V. A. Ushakov, O. A. Stonkus, I. Z. Ismagilov, M. A. Kerzhentsev and Z. R. Ismagilov, *Kinet. Catal.*, 2017, **58**, 610 (*Kinet. Katal.*, 2017, **58**, 623).
25 M. M. Makri, M. A. Vasiliades, K. C. Petallidou and A. M. Efstathiou, *Catal. Today*, 2016, **259**, 150.
26 Q. Wang, F. Du, Y. Hou, Y. Zhang, M. Cui and Y. Zhang, *Ceram. Int.*, 2021, **47**, 33057.
27 B. Bulfin, L. Hoffmann, L. de Oliveira, N. Knoblauch, F. Call, M. Roeb, C. Sattler and M. Schmücker, *Phys. Chem. Chem. Phys.*, 2016, **18**, 23147.
28 M. A. Vasiliades, M. M. Makri, P. Djinović, B. Erjavec, A. Pintar and A. M. Efstathiou, *Appl. Catal., B*, 2016, **197**, 168.
29 P. N. Kechagiopoulos, S. D. Angeli and A. A. Lemonidou, *Appl. Catal., B*, 2017, **205**, 238.
30 A. I. Osman, *Chem. Eng. Technol.*, 2020, **43**, 641.
31 S. Chen, J. Zaffran and B. Yang, *ACS Catal.*, 2020, **10**, 3074.

Received: 24th June 2021; Com. 21/6596